Water Science & Technology

IWA PUBLISHING

Water Science & Technology Vol 84 No 9, 2446 doi: 10.2166/wst.2021.434

Highly efficient scavenging of Cr(VI) by two-dimensional titanium carbide nanosheets: kinetics, isotherms and thermodynamics analysis

Yinzhi Lv[a], Kaikai Chang[b], Hui Wu[a], Ping Fang[a], Chaogui Chen[a] and Qing Liao[a,*]

[a] College of Chemistry and Chemical Engineering, Shaoxing University, Shaoxing, Zhejiang 312000, China
[b] Shaoxing Yigao Testing Technology Co., Ltd, Shaoxing, Zhejiang 312000, China
*Corresponding author. E-mail: lq0318@usx.edu.cn

KC, 0000-0001-6718-7437; PF, 0000-0001-9437-2531; QL, 0000-0002-1974-4697

ABSTRACT

In this study, two-dimensional (2D) MXene material ($Ti_3C_2T_x$) was employed to investigate its potentials toward the Cr(VI) removal in aqueous system by batch experiments. Characterization techniques such as SEM-EDS, HRTEM, XRD, FI-TR and XPS were used to analyze the structure and interaction of $Ti_3C_2T_x$ before and after Cr(VI) adsorption. The results indicated that the layered structure of $Ti_3C_2T_x$ had unique surface functional properties and abundant active sites, such as –OH, Ti–O, C = O, which exhibited high adsorption capacity for Cr(VI) removal. The Cr(VI) adsorption capacity by $Ti_3C_2T_x$ decreased with the increase of pH, and its maximum value can reach 169.8 mg/g at pH = 2.0. The adsorption kinetic was well-explained by a pseudo-second-order kinetic, indicating that chemical interaction played a dominant role in the adsorption of Cr(VI) on $Ti_3C_2T_x$. Meanwhile, the isotherm data was calculated to conform to the Freundlich isotherm model. Thermodynamic analysis indicated that the adsorption process of Cr(VI) on $Ti_3C_2T_x$ was a spontaneous endothermic process. These experimental results revealed that $Ti_3C_2T_x$ had tremendous potential in heavy metals adsorption from aqueous solutions.

Key words: adsorption, Cr(VI), heavy metals, $Ti_3C_2T_x$, two-dimensional

HIGHLIGHTS

- Novel Two-dimensional titanium carbide nanosheets ($Ti_3C_2T_x$ MXene) were employed for Cr(VI) scavenging.
- $Ti_3C_2T_x$ MXene exhibited high adsorption ability for the Cr(VI) removal, namely 169.8 mg/g at pH = 2.0.
- The adsorption of Cr(VI) on $Ti_3C_2T_x$ MXene is a multilayer adsorption and spontaneous endothermic process.
- The chemical interaction played a dominant role in the Cr(VI) removal by $Ti_3C_2T_x$ MXene.

INTRODUCTION

Chromium contamination arises from several industries, such as leather tanning, stainless steels, pigments, textiles (Xu *et al.* 2011; Hoang *et al.* 2020), and so on. The trivalent form and hexavalent form of chromium are the usual valence states, of which hexavalent chromium is more toxic than trivalent chromium and is the main cause of pollution. Chromate is limited to be absorbed by aquifer minerals due to it having negative charges; as a result, chromate can move more easily in groundwater and is absorbed in the human body by bioaccumulation (Hong *et al.* 2008). It seriously influences human beings' health, owing to its carcinogenicity and destructive effects on the respiratory system (Wise *et al.* 2006; Anandkumar & Mandal 2011). According to the World Health Organization (WHO) requirements, the maximum concentration of Cr(VI) in drinking water should not exceed 0.05 mg/L (Miretzky & Cirelli 2010). Currently, the methods for the removal of Cr(VI) include chemical reduction (Park *et al.* 2005), adsorption (Karthikeyan & Meenakshi 2019), oxidation (Ouejhani *et al.* 2008), photocatalysis (Mao *et al.* 2020; Preethi *et al.* 2020), reverse osmosis (Das *et al.* 2006) and ion exchange (Xing *et al.* 2007). Among these treatment methods, the adsorption technique gets a lot of attention because of its simplicity, environmental friendliness and high efficiency. Adsorption materials, such as activated carbon (Chen *et al.* 2020), metal organic frameworks (MOF) (Ha *et al.* 2016; Alqadami *et al.* 2018), humic acid-iron-pillared bentonite (Xu *et al.* 2020), zeolite (Li *et al.* 2021) and cross-linked cyclodextrin polymer (CDP) (Wang *et al.* 2021) have been studied extensively. However, these adsorption

materials are fabricated by multiple-step, complex procedures, or have less functional groups on the surface. As a result, their low efficiency of adsorption, highly cost and stability issues restrict the practical application for the Cr(VI) removal. Therefore, it is important to develop an economic and effective method to solve these practical issues.

In recent years, MXene has actively appeared on many areas owing to its remarkable abilities, such as hydrophilicity, thermostability, flexibility and electroconductibility (Du *et al.* 2019). MAX is the precursor of MXenes, where M is an early transition metal (e.g., Nb or Ti). A is an IVA/IIIA element (e.g., Al, Si, Sn and so on), and X is carbon or nitrogen. MXenes can be achieved by etching the A levels, and the chemical formular is $M_{n+1}X_nT_x$. T_x is a surface functional group (e.g., -F, -OH or -O). As an adsorbent, MXene exhibits high adsorption capacity and adsorption efficiency, due to its special structure, enormous surface area and plenty of functional groups on the surface (Li *et al.* 2019). For example, Jun *et al.* reported that MXene had high capacity for dyes adsorption (~140 mg/g) (Jun *et al.* 2020a). They also used MXene to remove Ba^{2+} and Sr^{2+}, and the adsorption capacity could reach 180 mg/g and 225 mg/g, respectively (Jun *et al.* 2019a). Zhang *et al.* reported that carboxyl functionalized MXene nanosheets showed superior adsorption capacity for Eu(III) and U(VI) ions, which can reach 97.1 mg/g and 344.8 mg/g (Zhang *et al.* 2020). Nevertheless, to our knowledge, there are few comprehensive systematic studies for the Cr(VI) removal by $Ti_3C_2T_x$ MXene.

In this paper, $Ti_3C_2T_x$ MXene was used to remove Cr(VI) and the adsorption behavior of Cr(VI) on $Ti_3C_2T_x$ MXene was investigated systematically. The chemical compositions, lattice structure, micromorphology and surface functional groups of $Ti_3C_2T_x$ MXene were characterized by SEM-EDS, XRD, HRTEM, FI-TR and XPS in detail. The effects of solution pH, contacting time, reaction temperature, initial concentration and adsobent dosage for the Cr(VI) removal by $Ti_3C_2T_x$ MXene were investigated in detail to evaluate the adsorption performance. In addition, the adsorption kinetics and thermodynamic data were also investigated to comprehend the mechanism of adsorption behaviors. Notably, $Ti_3C_2T_x$ MXene exhibited excellent adsorption performance for the Cr(VI) removal, and it had a good directive significance for eliminating Cr(VI) in the water environment.

MATERIALS AND METHODS

Materials

$Ti_3C_2T_x$ MXene was synthesized by etching Al from the Ti_3AlC_2 using lithium fluoride (LiF) and hydrochloric acid (HCl) (Alhabeb *et al.* 2017; Ding *et al.* 2017). In brief, the etchant was prepared by adding a certain amount of LiF and HCl with continuous stirring for 5 min. Then, the Ti_3AlC_2 powder was gradually added into the above etchant with 24 h stirring, and the mixture was washed with deionized water to remove reaction products and residual acid until pH 6–7 was achieved. Subsequently, the obtained powders were sonicated and vacuum-dried at room temperature for 24 h to produce the final product.

Characterization of $Ti_3C_2T_x$ MXene

Fourier transform infrared spectra (FT-IR) were recorded on a NEXUS spectrometer to estimate the surface functional groups. Transmission electron microsopy (HRTEM, JEM-2100F) and scanning electron microscopy (SEM, JSM-6360LV) were used to observe the morphology and structure of $Ti_3C_2T_x$ MXene, respectively. X-ray diffraction (XRD, Empyrean, Cu Kα radiation) was used to characterize the phase structure of $Ti_3C_2T_x$ MXene. AUV-vis spectrophotometer was used to measure the residual concentrations of Cr(VI). An energy-dispersive spectrometer (EDS) was used to characterize the elements existing on the $Ti_3C_2T_x$ after adsorption. X-ray photoelectron spectra (XPS) was recorded on a Thermo Scientific K-Alpha to analyze the material composition and binding energies.

Batch experiments

All batch experiments for the Cr(VI) removal on $Ti_3C_2T_x$ proceeded in 100.0 mL glass vials with a rubber cap. During the adsorption experiment, we adopted different parameters, including the solution pH value, reaction time, initial concentration of Cr(VI), temperature and the dosage of adsorbent. In order to make sure the reaction was fully completed, all the adsorption processes were over 24 h. To figure out the effect of solution pH, the Cr(VI) solution was adjusted to a constant pH of 2.12, 3.09, 4.04, 5.04, 6.01, 6.93, 7.94 and 9.06 with 0.2 g/L of $Ti_3C_2T_x$ and 30 mg/L of Cr(VI). To explore the influence of reaction time, we took 0.2 g/L of $Ti_3C_2T_x$ to adsorb 50 mg/L of Cr(VI) and the contact time was sustained for 30 h. To examine the effect of Cr(VI) initial concentration, different concentrations of Cr(VI) were examined under the same reaction condition (the adsorbent is 0.2 g/L). To investigate the impact of $Ti_3C_2T_x$ dosage, the $Ti_3C_2T_x$ dosage was separated into 0.05 g/L,

0.1 g/L, 0.15 g/L, 0.2 g/L, 0.25 g/L and 0.3 g/L at T = 303 K. For all experiments, the glass vials were sealed by rubber caps, and took place in a table concentrator, which set the rotation speed at 220 rpm. When the reaction finished, we separated the aqueous phase from the solid phase by using 0.22-μm polyethersulfone membrane filters. To improve the tested process of the Cr(VI) concentrations, we used 1 mL supernatant, 1 mL mixed acid (phosphoric acid and sulfuric acid) and 3 mL dipenylsemicarbarize to dilute into 25.0 mL of colorimetric tube. The concentration of Cr(VI) was tested by UV-vis spectrophotometer and the wave length was set at 540 nm. There was a blank control group under the same conditions without adsorbent.

$$\text{Adsorption capacity (mg/g)} = \frac{C_0 - C_e}{m} \times V \quad (1)$$

$$\text{Removal percentage (\%)} = \frac{C_0 - C_e}{C_0} \times 100\% \quad (2)$$

where C_0 is initial concentrations of Cr(VI), C_e is equilibrium concentrations of Cr(VI), V is solution volume (L), m is mass of $Ti_3C_2T_x$ MXene (mg). All experimental data were carried out to the average of duplicate or triplicate determinations. The relative errors of the data were about 5%.

RESULTS AND DISCUSSION

Characterization

The surface morphology, lattice structure and functional groups of $Ti_3C_2T_x$ MXene before and after Cr(VI) adsorption were analyzed by HRTEM, SEM, XRD, FTIR and SEM-EDS, as shown in Figure 1, Figure S1 (Supporting Information) and Figure 2. Figure 1(a) and 1(c) and Figure S1 present the $Ti_3C_2T_x$ MXene SEM and HRTEM image before adsorption. It can be seen that $Ti_3C_2T_x$ MXene possessed a multi-nanolamellar stacking structure with a few layers like grapheme (Avila *et al.* 2014). After adsorbing Cr(VI), there was black shadows existing on the surface of $Ti_3C_2T_x$ MXene (Figure 1(b) and 1(d)), which indicated that Cr(VI) had been successfully adsorbed on the $Ti_3C_2T_x$ MXene. Figure 1(e) presented the XRD of Ti_3AlC_2, $Ti_3C_2T_x$ before and after Cr(VI) adsorption. The characteristic peaks of Ti_3AlC_2 at 9.58°, 19.14°, 34.01° and 38.98° were the (002), (004), (101) and (104) plane (Tran *et al.* 2021). After being etched by HCl-LiF, the Ti_3AlC_2 characteristic peak of Al layers at 39° disappeared, showing that $Ti_3C_2T_x$ MXene was successfully prepared. Meanwhile, the $Ti_3C_2T_x$ MXene of (002) plane was shifted down to 8.84°, the d-spacing of $Ti_3C_2T_x$ MXene became larger than Ti_3AlC_2 (Mu *et al.* 2018). However, the characteristic peaks were basically the same after adsorbing Cr(VI), which indicated the structure of $Ti_3C_2T_x$ MXene was stable during the adsorption process. Figure 1(f) showed the FTIR of $Ti_3C_2T_x$ MXene before and after Cr(VI) adsorption. It can be seen that the distinctive peaks at 3,436, 1,631 and 805 cm^{-1} were corresponding to the –OH stretching vibrations of $Ti_3C_2T_x$ MXene, intimating that there were water moieties and –OH group existing on the surface of the adsorbent (Shahzad *et al.* 2019). The vibration band at 547 cm^{-1} presented the Ti–O stretching bands (Karthikeyan *et al.* 2021a, 2021b), and the adsorption peak at 1629 and 1400 cm^{-1} belonged to the C = O and C–O stretching vibration of the carboxyl group (Dong *et al.* 2019). After Cr(VI) adsorption, the peak at 3,436 cm^{-1} was shifted to 3,430 cm^{-1}, indicating the hydrogen bonds were formed between the $Ti_3C_2T_x$ MXene and Cr(VI). Similarly, the Ti–O, C = O and –OH peaks area of $Ti_3C_2T_x$ MXene tended to a lower peak area, revealing that there was an interaction between the $Ti_3C_2T_x$ MXene material and Cr(VI). Figure 2 showed the SEM-EDS of $Ti_3C_2T_x$ MXene after Cr(VI) adsorption. Obviously, the elements C, Ti, F, O and Cr were detected, and they were distributed uniformly. These results exhibited that Cr(VI) was successfully adsorbed onto $Ti_3C_2T_x$ MXene with surface interactions, which were consistent with the HRTEM result in Figure 1(d).

Figure 3 presented the XPS spectra of $Ti_3C_2T_x$ before and after Cr(VI) adsorption. From Figure 3(a), it can be seen that the elements of Ti, C, O, F were detected before reaction. After Cr(VI) adsorption, the additional peaks of Cr at ~578 eV and ~588 eV were detected, indicating that Cr(VI) had been successfully adsorbed onto $Ti_3C_2T_x$ MXene. The results were consistent with TEM and SEM-EDS in Figure 1. In order to acquire more information about the elemental chemical states before and after Cr(VI) adsorption, high resolution XPS spectra of Ti2p, C1s, O1s, F1s and Cr2p were analyzed. For the spectra of Ti2p (Figure 3(b)), the peaks were located at 454.7 eV, 455.7 eV, 457.4 eV, 461.1 eV, 462.3 eV and 465.4 eV respectively. The peaks at 454.7 eV and 461.1 eV were associated with Ti – C, while the peaks centered at 455.7 eV, 457.4 eV, 462.3 eV and 465.4 eV can be assigned as Ti^{2+} oxide, Ti ions with reduced charge state (Ti_xO_y), Ti^{3+} oxide and Ti – O – F (Peng *et al.* 2016; Ding *et al.* 2017; Elumalai *et al.* 2020). The high-resolution O1s spectrum (Figure 3(c)) can be appropriately fitted to four peaks at

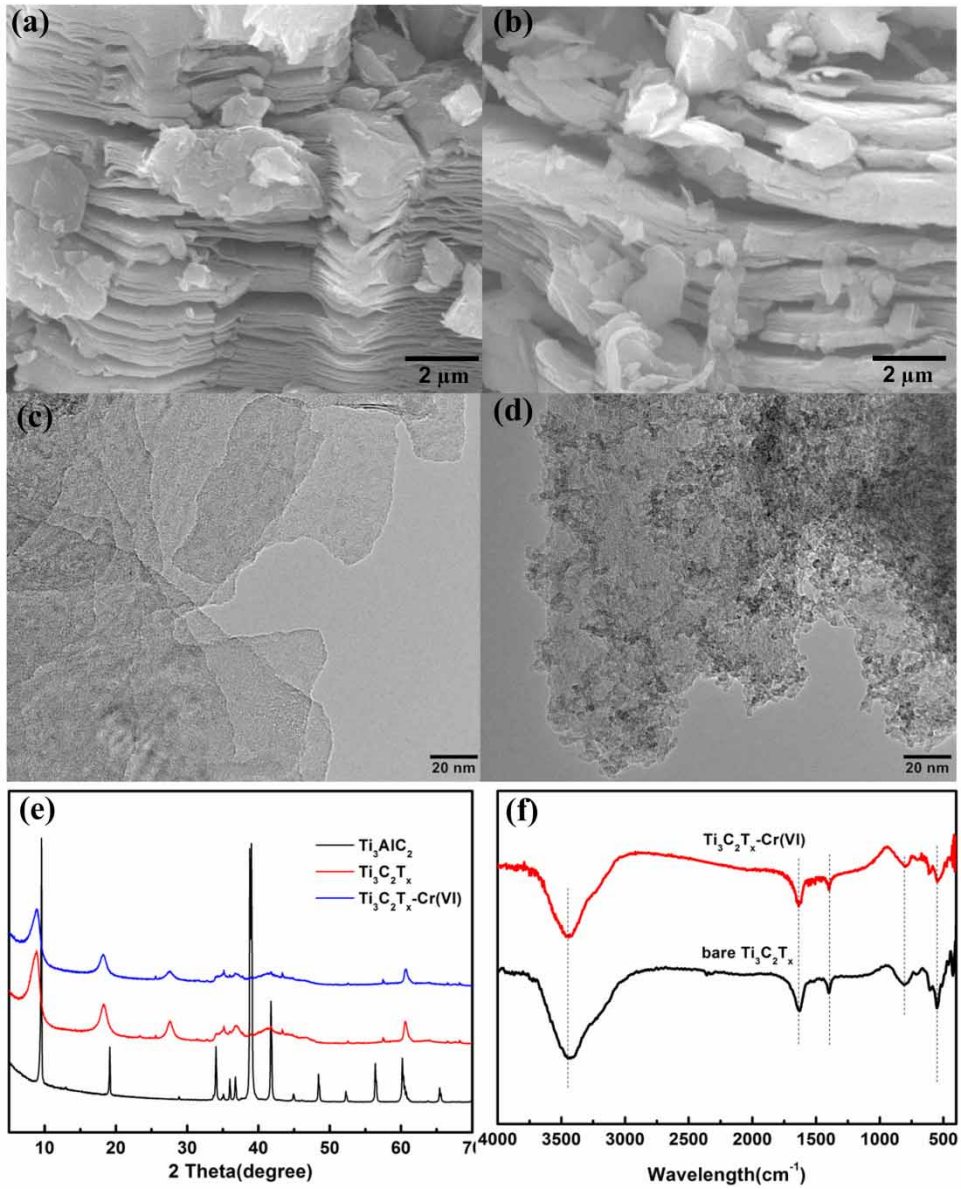

Figure 1 | (a) SEM image of the $Ti_3C_2T_x$; (b) SEM image of $Ti_3C_2T_x$ after adsorption of Cr(VI); (c) HRTEM image of $Ti_3C_2T_x$; (d) HRTEM image of $Ti_3C_2T_x$ after adsorption of Cr(VI); (e) XRD pattern of Ti_3AlC_2, $Ti_3C_2T_x$ before and after Cr(VI) adsorption; (f) FT-IR spectra of $Ti_3C_2T_x$ before and after Cr(VI) adsorption.

529.5 eV, 530.0 eV, 531.7 eV and 533.2 eV. The peaks located at 529.5 and 530.0 eV were ascribed to surface adsorbed O species and Ti–O–Ti, and the peak centered at 531.5 and 533.2 eV were attributed to Ti–OH and C–OH species (Peng *et al.* 2016). The C1s spectra of $Ti_3C_2T_x$ (Figure 3(d)) was fitted by four peaks at 281.7 eV, 282.1 eV, 284.7 eV and 286.2 eV, corresponding to C – Ti, C – Ti-O, C – C and C – O, respectively (Rakhi *et al.* 2015; Peng *et al.* 2016). Binding energies of F1s (Figure 3(e)) at 685.2 and 686.5 eV were ascribed to F – Ti and F – C, respectively (Ding *et al.* 2017). Notably, the peaks of Ti2p, C1s, O1s, F1s were obviously shifted to some extent after adsorption, reflecting the strong binding affinity and interaction between Cr(VI) and $Ti_3C_2T_x$ MXene. Similarly, the spectra of Cr 2p (Figure 3(f)) can be divided into three peaks at around 577.2 eV, 578.5 eV, 587.4 eV and 588.1 eV. The peaks centered at 577.2 and 588.1 eV were attributed to the peak centered at 531.5 and 533.2 eV were attributed to Cr(VI), and the peaks located at 578.5 and 587.4 eV were ascribed to Cr(III) and Cr_2O_3, respectively (Wu *et al.* 2020; Karthikeyan *et al.* 2021a, 2021b). These results implied Cr(VI) was moderately converted to Cr(III), because of an additional feature of $Ti_3C_2T_x$. And similar findings have also been reported (Karthikeyan *et al.* 2021a, 2021b).

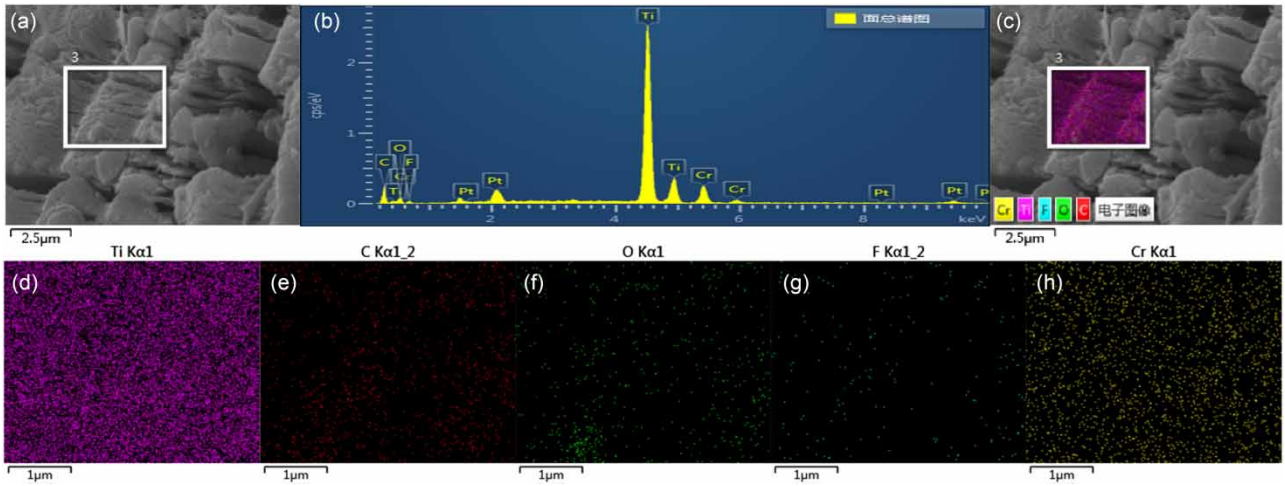

Figure 2 | SEM-EDS results of $Ti_3C_2T_x$ reacted with Cr(VI).

Effects of pH and sorbent dosage

The solution pH is a critical condition for Cr(VI) removal since it can affect the physicochemical properties of both the adsorbate and adsorbent (Karthikeyan *et al.* 2021a, 2021b). Therefore, the Cr(VI) adsorption on $Ti_3C_2T_x$ MXene at different pH values was investigated, to figure out the influence of pH on adsorption. Normally, the Cr(VI) ions exist in several forms in aqueous solution varied with different pH. When the pH value is between 2.0 and 6.0, the main form of Cr(VI) is $HCrO_4^-$ and $Cr_2O_7^{2-}$. The CrO_4^{2-} is predominant while the pH value is greater than 6.0, whereas H_2CrO_4 mainly exists at pH <1.0. The pH value was ranged from 2.12 to 9.06 using a 0.1 mol/L HCl/NaOH aqueous solution. As shown in Figure 4(a), the adsorption of Cr(VI) on $Ti_3C_2T_x$ MXene decreased persistently with the increase of pH value. At pH = 2.12, the adsorption capacity of Cr(VI) on $Ti_3C_2T_x$ MXene was 110.25 mg/g. However, it was only 21.86 mg/g when pH = 9.06 under the similar conditions. The reason for this phenomenon was that the surface charge was affected by solution pH and the adsorption of Cr(VI) was electrostatic in nature (Jun *et al.* 2020b). Under acidic conditions, the functional groups on $Ti_3C_2T_x$ MXene would be protonated to generate positive charge sites, leading to stronger electrostatic attraction to negatively charged Cr(VI) ions. However, the degree of protonation decreased and the OH^- increased with the increase of pH value. The competition between OH^- ions and negatively charged Cr(VI) ions resulted in the decrease of adsorption capacity. In previous investigations, Saravanan *et al.* explored the influence of pH on the adsorption of Cr(VI) on magnetic nanoparticles coated with mixed fungal biomass (Saravanan *et al.* 2021). Feng *et al.* discussed the impact of pH on MXene/PEI functionalized sodium alginate aerogel for Cr(VI) removal (Feng *et al.* 2021). Tangtubtim *et al.* studied the influence of pH on Cr(VI) removal with polyethyleneimine-carbamate linked pineapple leaf fiber (Tangtubtim & Saikrasun 2019). And similar findings have also been reported by them.

Figure 4(b) shows the influence of sorbent dosage on Cr(VI) removal by $Ti_3C_2T_x$ MXene. It can be seen that the adsorption capacity was decreasing gradually with adding sorbent dosage. However, the tendency of the removal efficiency was totally opposite. When the sorbent dosage was 0.05 g/L, the adsorption capacity and the removal efficiency of Cr(VI) on $Ti_3C_2T_x$ MXene were 138.42 mg/g and 23.01%, respectively. However, the adsorption capacity reduced to 103.86 mg/g and the removal efficiency of Cr(VI) increased to 100% when the sorbent dosage was 0.30 g/L. The reason for this phenomenon was the removal ratio and the amount of unoccupied adsorption sites. As the dosage of sorbent increased, the Cr(VI) diffusion rate and the reactive sites of adsorption onto $Ti_3C_2T_x$ MXene were reduced at high dosage. Jun *et al.* and Li *et al.* explored the effects of adsorbent dose on lead by GO and MOF, and Ni(II) by porous hexagonal boron nitride, respectively (Jun *et al.* 2019b; Li *et al.* 2020), and similar findings have been reported by them.

Adsorption kinetics of Cr(VI) onto MXene

Figure 5(a) depicted the Cr(VI) adsorption on $Ti_3C_2T_x$ as a function of contact time. It was shown that the Cr(VI) adsorption increased quickly at the first 10 h, and then increased slightly until equilibrium (20 h). In order to explore the controlling mechanism of the Cr(VI) removal by $Ti_3C_2T_x$, and possible rate-determining steps such as chemical reduction reaction and mass transport processes, three kinetic models, namely, the pseudo-first-order model, pseudo-second-order model and

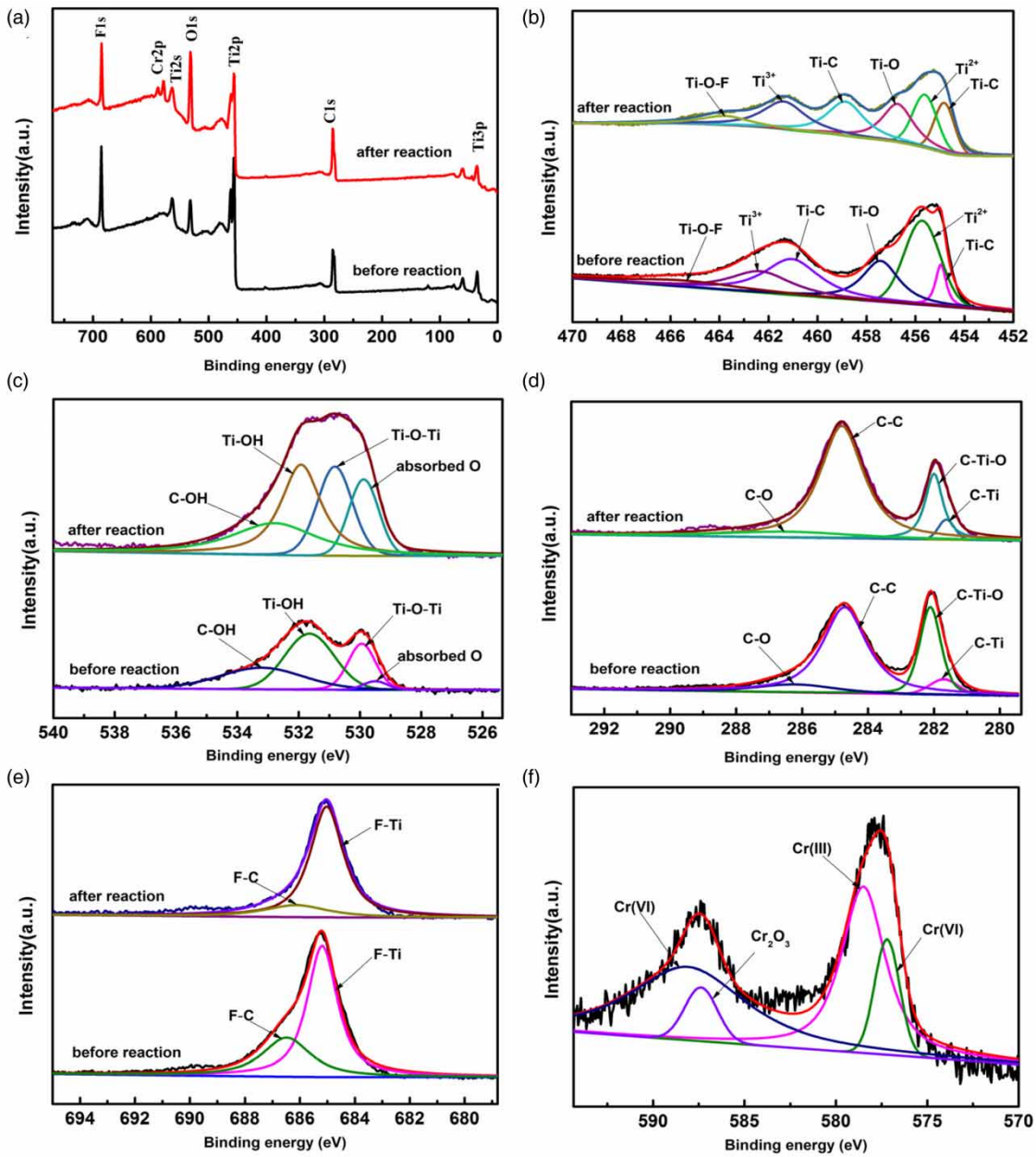

Figure 3 | (a) XPS surveys for $Ti_3C_2T_x$ before and after Cr(VI) adsorption; the high resolution XPS spectra for (b) Ti2p (c) O1s (d) C1s (e) F1s (f) Cr2p.

intra-particle diffusion model were applied to fit the experimental data. The equations are as follows (Wu *et al.* 2020):

$$\ln(q_e - q_t) = \ln q_e - k_1 t \tag{3}$$

$$\frac{t}{q_t} = \frac{1}{k_2 q_e^2} + \frac{t}{q_e} \tag{4}$$

$$q_t = k_d \times t^{1/2} + I \tag{5}$$

where q_t is the value of TiC_2T_x sorption Cr(VI) at time t (h), q_e is the amount of $Ti_3C_2T_x$ sorption Cr(VI) achieved at equilibrium, $k_1(h^{-1})$, $k_2(g{\cdot}h^{-1}{\cdot}\ mg^{-1})$ and $k_d(h^{-1})$ is the constant model. Figure 5(b)–5(d) presented the fitting results by three

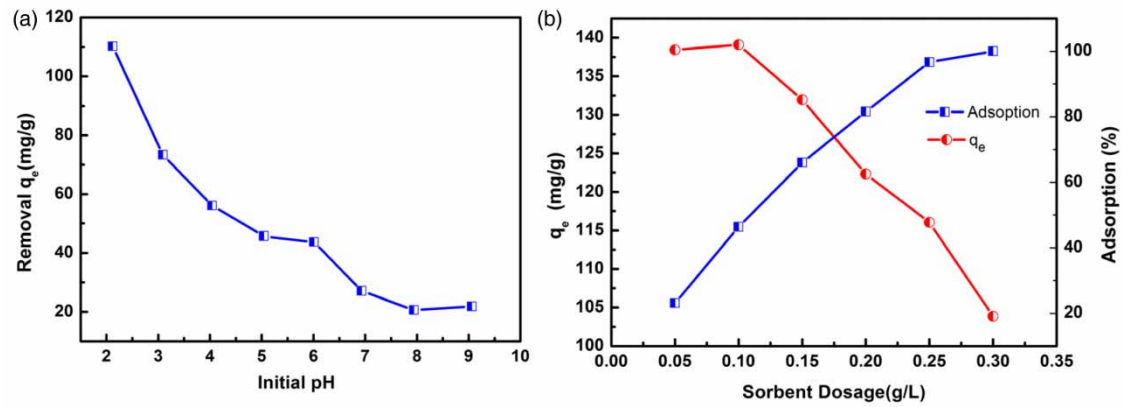

Figure 4 | (a) Effects of initial pH to Cr(VI) adsorption capacity; (b) effect of $Ti_3C_2T_x$ dosage on the adsorption capacity and adsorption percentage of Cr(VI).

kinetic models, and the corresponding parameters are rendered in Table S1 (Supporting Information). From Table S1, it can be seen that the pseudo-second-order dynamics model was more correlated with the adsorption of Cr(VI) on $Ti_3C_2T_x$ ($R^2 = 0.997$), and the experimental value of the adsorption capacity (125.32 mg/g) is very close to the theoretical value (128.04 mg/g). These results indicated that the Cr(VI) adsorption process by $Ti_3C_2T_x$ comprised the sharing or transfer of electrons, which indicating that chemisorption was more dominant than physisorption (Ho & McKay 1999).

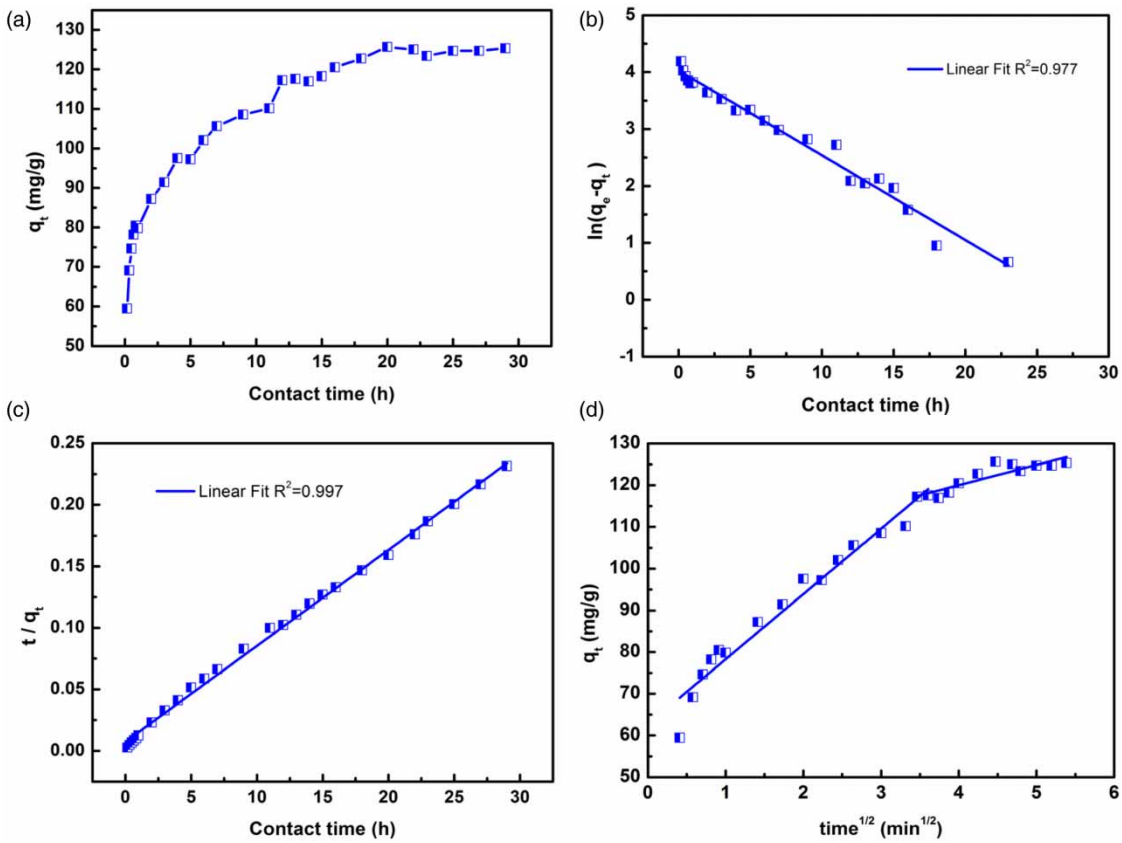

Figure 5 | (a) Adsorption capacity of Cr(VI) on $Ti_3C_2T_x$ as a function of contact time (b) pseudo-first-order model (c) pseudo-second-order model (d) intra-particle diffusion model.

Adsorption isotherms and thermodynamic study

Studying the adsorption isotherm not only can figure out the relation of the adsorbent and adsorbate, but also explore the change of adsorption capacity with temperature (Zhang *et al.* 2020). Figure 6(a) shows the adsorption isotherm of Cr(VI) removal by $Ti_3C_2T_x$ at T = 303 K, 318 K, 333 K, respectively. As observed, the amount of Cr(VI) adsorbed by $Ti_3C_2T_x$ increased with the rise of temperature, uncovering the Cr(VI) adsorption process by $Ti_3C_2T_x$ was an endothermic procedure. At T = 303 K, the amount of Cr(VI) adsorbed by $Ti_3C_2T_x$ was 125.3 mg/g, while it can reach 158.1 mg/g at T = 333 K under the similar conditions. In order to pursue the interaction behavior of Cr(VI) removal by $Ti_3C_2T_x$ further, we used three isotherm models, namely the Langmuir model, Freundlich model and Temkin model to fit the adsorption data. The equations are as follows (Wu *et al.* 2020):

$$\text{Langmuir model: } \frac{1}{q_e} = \frac{1}{q_{\max}} + \frac{1}{b \times q_{\max}} \cdot \frac{1}{C_e} \tag{6}$$

$$\text{Freundlich model: } \lg q_e = \lg K_F + n \lg C_e \tag{7}$$

$$\text{Temkin model: } q_e = K_T \times \ln f + K_T \times \ln C_e \tag{8}$$

where q_e is amounts of adsorption equilibrium; $q_{\max}$ is amounts of the maxium adsorption; C_e is Cr(VI) concentrations of adsorption equilibrium; b, K_F, n, f is the corresponding constant. Normally, the Langmuir model is used to analyze the adsorption behavior based on homogenous sites with monolayer adsorption. The Freundlich model was employed to explain the heterogeneous surface through multilayer adsorption, and the Temkin model was to evaluate the adsorbent-adsorbate interactions (Yousef *et al.* 2011; Tangtubtim & Saikrasun 2019). From Figure 6(b)–6(d) and Table S2, it can be seen that the

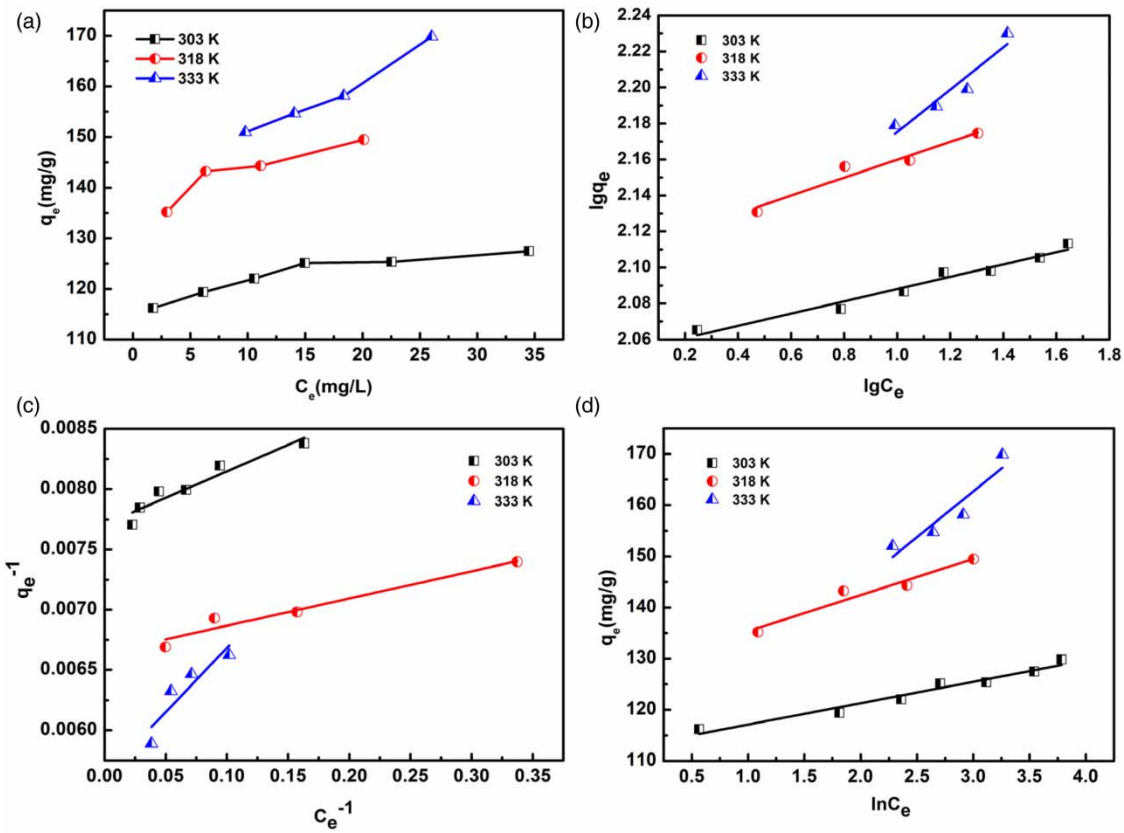

Figure 6 | (a) Adsorption isotherms of Cr(VI) on $Ti_3C_2T_x$ at different temperatures; Equilibrium adsorption isotherms fitted by (b) Freundlich model (c) Langmuir model (d) Temkin model at three different temperatures.

Freundlich model had a better correlation for the Cr(VI) adsorption on $Ti_3C_2T_x$. These results implied that the adsorption of Cr(VI) onto MXene was multilayer adsorption.

In order to explore the thermal properties of the adsorption process, several thermodynamic parameters (ΔG^θ, ΔH^θ, ΔS^θ) were calculated. They were calculated by Equations (9)–(11):

$$K_d = \frac{C_0 - C_e}{C_e}\frac{V}{m} \tag{9}$$

$$\ln K_d = \frac{\Delta S^\theta}{R} - \frac{\Delta H^\theta}{RT} \tag{10}$$

$$\Delta G^\theta = \Delta H^\theta - T\Delta S^\theta \tag{11}$$

where T represents the temperature, K_d represents distribution coefficient($mL \cdot g^{-1}$), $R = 8.314\ J \cdot mol^{-1} \cdot K^{-1}$. The relevant curves are depicted in Figure 7, and values of thermodynamic parameters for the adsorption of Cr(VI) on $Ti_3C_2T_x$ are listed in Table S3. The value of ΔH^θ and ΔS^θ were positive, indicating that the adsorption process was endothermic and the reaction system increased randomness. The negative value of ΔG^θ indicated that the adsorption procedure of Cr(VI) on $Ti_3C_2T_x$ was a spontaneous chemical process. This phenomenon reflected that (I) the boundary layer of adsorbent was thinner with the temperature persistently increasing; (II) the diffusion rate of Cr(VI) on $Ti_3C_2T_x$ increased; (III) the raised of the number of adsorbent activate sites, and the high temperature was beneficial to the adsorption process (Mirsoleimani-azizi *et al.* 2018).

CONCLUSIONS

In conclusion, we comprehensively studied and characterized $Ti_3C_2T_x$ by SEM, TEM, XRD, FI-TR, SEM-EDS and XPS. The effect of pH, sorbent dosage, contact time, initial concentration and temperature were also studied systematically. The results exhibited that the adsorption of Cr(VI) on $Ti_3C_2T_x$ was in favor of the low pH. At pH = 2.0, the adsorption capacity for Cr(VI) removal by $Ti_3C_2T_x$ can reach 169.8 mg/g. The adsorption kinetics revealed that the pseudo-second-order kinetic was more appropriate than the pseudo-first-order model, indicating that chemisorption was more dominant than physisorption. As for thermodynamics analysis, the adsorption of Cr(VI) on $Ti_3C_2T_x$ was better fitted with the Freundlich model, implying the Cr(VI) removal by $Ti_3C_2T_x$ was multilayer adsorption. Furthermore, the adsorption of Cr(VI) on $Ti_3C_2T_x$ was a spontaneous endothermic process based on the Gibbs free energy change (ΔG^θ), standard enthalpy change(ΔH^θ) and standard entropy change (ΔS^θ). In summary, $Ti_3C_2T_x$ MXene could be an outstanding adsorbent in the removal of heavy metals in aqueous solutions.

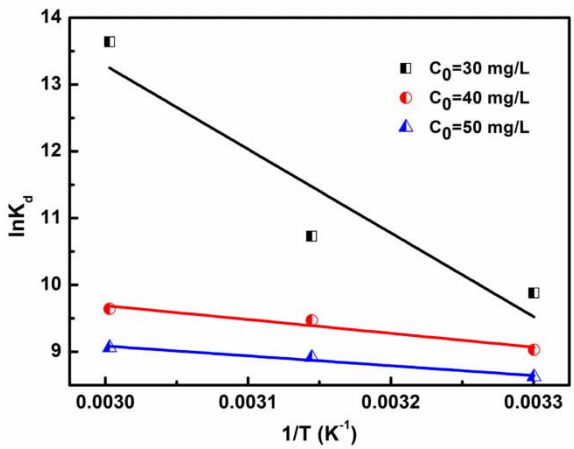

Figure 7 | The linear plot of $\ln K_d$ versus 1/T (K^{-1}) for Cr(VI) adsorption on $Ti_3C_2T_x$.

ACKNOWLEDGEMENTS

We gratefully acknowledge the funding from Scientific Research Fund (no. 20175003, 2015LG1004) in Shaoxing University. We also sincerely thank the young and middle aged academic cadres from Shaoxing University.

DATA AVAILABILITY STATEMENT

Data cannot be made publicly available; readers should contact the corresponding author for details.

REFERENCES

Alhabeb, M., Maleski, K., Anasori, B., Lelyukh, P., Clark, L., Sin, S. & Gogotsi, Y. 2017 Guidelines for synthesis and processing of two-dimensional titanium carbide ($Ti_3C_2T_x$ MXene). *Chem. Mater.* **29**, 7633–7644.

Alqadami, A., Naushad, M., Alothman, Z. & Ahamad, T. 2018 Adsorptive performance of MOF nanocomposite for methylene blue and Malachite Green dyes: kinetics, isotherm and mechanism. *J. Environ. Manage.* **223**, 29–36.

Anandkumar, J. & Mandal, B. 2011 Adsorption of chromium(VI) and Rhodamine B by surface modifified tannery waste: kinetic, mechanistic and thermodynamic studies. *J. Hazard. Mater.* **186**, 1088–1096.

Avila, M., Burks, T., Akhtar, F., Gothelid, M., Lansaker, P., Toprak, M., Muhammed, M. & Uheida, A. 2014 Surface functionalized nanofibers for the removal of chromium(VI) from aqueous solutions. *Chem. Eng. J.* **245**, 201–209.

Chen, H., Zhang, Z., Zhong, X., Zhuo, Z., Tian, S., Fu, S., Chen, Y. & Liu, Y. 2020 Constructing MoS_2/Lignin- derived carbon nanocomposites for highly efficient removal of Cr(VI) from aqueous environment. *J. Hazard. Mater.* **408**, 124847.

Das, C., Patel, P., De, S. & DasGupta, S. 2006 Treatment of tanning effluent using nanofiltration followed by reverse osmosis. *Sep. Purif. Technol.* **50**, 291–299.

Ding, L., Wei, Y., Wang, Y., Chen, H., Caro, J. & Wang, H. 2017 A two-dimensional lamellar membrane: MXene nanosheet stacks. *Angew. Chem. Int. Ed.* **56**, 1825–1829.

Dong, Y., Sang, D., He, C., Sheng, X. & Lei, L. 2019 Mxene/alginate composites for lead and copper ion removal from aqueous solutions. *RSC Adv.* **9**, 29015–29022.

Du, Y., Yu, B., Wei, L., Wang, Y., Zhang, X. & Ye, S. 2019 Efficient removal of Pb(II) by $Ti_3C_2T_x$ powder modified with a silane coupling agent. *J. Mater. Sci.* **54**, 13283–13297.

Elumalai, S., Yoshimura, M. & Ogawa, M. 2020 Simultaneous delamination and rutile formation on the surface of $Ti_3C_2T_x$ MXene for copper adsorption. *Chem-Asian. J.* **15**, 7.

Feng, Y., Wang, H., Xu, J., Du, X., Cheng, X., Du, Z. & Wang, H. 2021 Fabrication of MXene/PEI functionalized sodium alginate aerogel and its excellent adsorption behavior for Cr(VI) and Congo Red from aqueous solution. *J. Hazard. Mater.* **416**, 125777.

Ha, N., Lefedova, O. & Ha, N. 2016 Theoretical study on the adsorption of carbon dioxide on individual and alkali-metal doped MOF-5s. *Russ. J. Phys. Chem. A.* **90**, 220–225.

Ho, Y. & McKay, G. 1999 Pseudo-second order model for sorption processes. *Process Biochem.* **34**, 451–465.

Hoang, L., Nguyen, T., Van, H., Hoang, T., Vu, X., Nguyen, T. & Ca, N. 2020 Cr(VI) removal from aqueous solution using a magnetite snail shell. *Water. Air. Soil. Poll.* **231**, 28.

Hong, H., Jiang, W., Zhang, X., Tie, L. & Li, Z. 2008 Adsorption of Cr(VI) on STAC modified rectorite. *Appl. Clay. Sci.* **42**, 292–299.

Jun, B., Park, C., Heo, J. & Yoon, Y. 2019a Adsorption of Ba^{2+} and Sr^{2+} on $Ti_3C_2T_x$ MXene in model fracking wastewater. *J. Environ. Manage.* **256**, 10994.

Jun, B., Kim, S., Kim, Y., Her, N., Heo, J., Han, J., Jang, M., Park, C. & Yoon, Y. 2019b Comprehensive evaluation on removal of lead by graphene oxide and metal organic framework. *Chemosphere* **231**, 82–92.

Jun, B., Heo, J., Taheri-Qazvini, N., Parke, C. & Yoon, Y. 2020a Adsorption of selected dyes on $Ti_3C_2T_x$ MXene and Al-based metal-organic framework. *Ceram. Int.* **46**, 2960–2968.

Jun, B., Her, N., Chang, M. & Yoon, Y. 2020b Effective removal of Pb(II) from synthetic wastewater using $Ti_3C_2T_x$ MXene. *Environ. Sci. Water Res.* **6**, 173–180.

Karthikeyan, P. & Meenakshi, S. 2019 In-situ fabrication of zirconium entrenched biopolymeric hybrid membrane for the removal of toxic anions from aqueous medium. *Int. J. Biol. Macromol.* **141**, 1199–1209.

Karthikeyan, P., Elanchezhiyan, S., Preethi, J., Talukdar, K., Meenakshi, S. & Park, C. 2021a Two-dimensional (2D) $Ti_3C_2T_x$ MXene nanosheets with superior adsorption behavior for phosphate and nitrate ions from the aqueous environment. *Ceram. Int.* **47**, 732–739.

Karthikeyan, P., Ramkumar, K., Pandi, K., Fayyaz, A., Meenakshi, S. & Park, C. 2021b Effective removal of Cr(VI) and methyl orange from the aqueous environment using two-dimensional (2D) $Ti_3C_2T_x$ MXene nanosheets. *Ceram. Int.* **47**, 3692–3698.

Li, S., Wang, L., Peng, J., Zhai, M. & Shi, W. 2019 Effifficient thorium(IV) removal by two dimensional Ti_2CT_x MXene from aqueous solution. *Chem. Eng. J.* **366**, 192–199.

Li, L., Chang, K., Fang, P., Du, K., Chen, C., Zhou, S., Shen, C., Linghu, W., Sheng, G., Haya, T. & Guo, X. 2020 Highly efficient scavenging of Ni(II) by porous hexagonal boron nitride: kinetics, thermodynamics and mechanism aspects. *Appl. Surf. Sci.* **521**, 146373.

Li, X., Wang, J., Guo, Y., Zhu, T. & Xu, W. 2021 Adsorption and desorption characteristics of hydrophobic hierarchical zeolites for the removal of volatile organic compounds. *Chem. Eng. J.* **411**, 128558.

Mao, W., Zhang, L., Wang, T., Bai, Y. & Guan, Y. 2020 Fabrication of highly efficient Bi_2WO_6/CuS composite for visible-light photocatalytic removal of organic pollutants and Cr(VI) from wastewater. *Front. Env. Sci. Eng.* **15**, 1–13.

Miretzky, P. & Cirelli, A. 2010 Cr(VI) and Cr(III) removal from aqueous solution by raw and modified lignocellulosic materials: a review. *J. Hazard. Mater.* **180**, 1–19.

Mirsoleimani-azizi, S., Setoodeh, P., Zeinali, S. & Rahimpour, M. 2018 Tetracycline antibiotic removal from aqueous solutions by MOF-5: adsorption isotherm, kinetic and thermodynamic studies. *J. Environ. Chem. Eng.* **6**, 6118–6130.

Mu, W., Du, S., Yu, Q., Li, X., Wei, H. & Yang, Y. 2018 Improving barium ions adsorption on two-dimensional titanium carbide by surface modification. *Dalton. T.* **47**, 8375–8381.

Ouejhani, A., Hellal, F., Dachraoui, M., Lalleve, G. & Fauvarque, J. 2008 Application of Doehlert matrix to the study of electrochemical oxidation of Cr(III) to Cr(VI) in order to recover chromium from wastewater tanning baths. *J. Hazard. Mater.* **157**, 423–431.

Park, D., Yun, Y., Jo, J. & Park, J. 2005 Mechanism of hexavalent chromium removal by dead fungal biomass of *Aspergillus niger*. *Water. Res.* **39**, 533–540.

Peng, C., Yang, X., Li, Y., Yu, H., Wang, H. & Peng, F. 2016 Hybrids of two-dimensional Ti_3C_2 and TiO_2 exposing{001} facets toward enhanced photocatalytic activity. *ACS Appl. Mater. Inter.* **8**, 6051–6060.

Preethi, J., Farzana, M., Rathinam, K., Vigneshwaran, S., Karthikeyan, P. & Meenakshi, S. 2020 Enhanced photocatalytic response of ZnO embedded chitosan/betacyclodextrin towards the detoxification of Cr(VI) under visible light. *Int. J. Biol. Macromol.* **147**, 867–876.

Rakhi, R., Ahmed, B., Hedhili, M., Anjum, D. & Alshareef, H. 2015 Effect of postetch annealing gas composition on the structural and electrochemical properties of Ti_2CT_x MXene electrodes for supercapacitor applications. *Chem. Mater.* **27**, 5314–5323.

Saravanan, A., Kumar, P., Govarthanan, M., George, C., Vaishnavi, S., Moulishwaran, B., Kumar, S., Jeevanantham, S. & Yaashikaa, P. 2021 Adsorption characteristics of magnetic nanoparticles coated mixed fungal biomass for toxic Cr(VI) ions in aquatic environment. *Chemosphere* **267**, 129226.

Shahzad, A., Nawaz, M., Moztahida, M., Jang, J., Tahir, K., Kim, J., Lim, Y., Vassiliadis, V., Woo, S. & Lee, D. 2019 $Ti_3C_2T_x$ MXene core-shell spheres for ultrahigh removal of mercuric ions. *Chem. Eng. J.* **368**, 400–408.

Tangtubtim, S. & Saikrasun, S. 2019 Adsorption behavior of polyethyleneimine-carbamate linked pineapple leaf fiber for Cr(VI) removal. *Appl. Surf. Sci* **467–468**, 596–607.

Tran, N., Ta, Q., Sreedhar, A. & Noh, J. 2021 $Ti_3C_2T_x$ MXene playing as a strong methylene blue adsorbent in wastewater. *Appl. Surf. Sci.* **537**, 148006.

Wang, M., Li, G., Xi, C., Jing, X., Wang, R., Liu, Q. & Cai, X. 2021 Facile preparation of cyclodextrin polymer materials with rigid spherical structure and flexible network for sorption of organic contaminants in water. *Chem. Eng. J.* **411**, 128489.

Wise, S., Holmes, A. & Wise, J. 2006 Particulate and soluble hexavalent chromium are cytotoxic and genotoxic to human lung epithelial cells. *Mutat. Res.* **610**, 2–7.

Wu, H., Li, L., Chang, K., Du, K., Shen, C., Zhou, S., Sheng, G., Linghu, W., Hayat, T. & Guo, X. 2020 Graphene oxide decorated nanoscale iron sulfide for highly efficient scavenging of hexavalent chromium from aqueous solutions. *J. Environ. Chem. Eng.* **8**, 103882.

Xing, Y., Chen, X. & Wang, D. 2007 Electrically regenerated ion exchange for removal and recovery of Cr(VI) from wastewater. *Environ. Sci. Technol.* **41**, 1439–1443.

Xu, X., Gao, B., Tang, X., Yue, Q., Zhong, Q. & Li, Q. 2011 Characteristics of cellulosic amine-crosslinked copolymer and its sorption properties for Cr(VI) from aqueous solutions. *J. Hazard. Mater.* **189**, 420–426.

Xu, H., Hu, X., Chen, Y., Li, Y., Zhang, R., Tang, C. & Hu, X. 2020 Cd(II) and Pb(II) absorbed on humic acid-iron-pillared bentonite: kinetics, thermodynamics and mechanism of adsorption. *Colloid. Surface. A.* **621**, 126005.

Yousef, R., El-Eswed, B. & Al-Muhtaseb, A. 2011 Adsorption characteristics of natural zeolites as solid adsorbents for phenol removal from aqueous solutions: kinetics, mechanism, and thermodynamics studies. *Chem. Eng. J.* **171**, 1143–1149.

Zhang, P., Wang, L., Du, K., Wang, S., Huang, Z., Yuan, L., Li, Z., Wang, H., Zheng, L., Chai, Z. & Shi, W. 2020 Effective removal of U(VI) and Eu(III) by carboxyl functionalized MXene nanosheets. *J. Hazard. Mater.* **396**, 122731.

First received 17 July 2021; accepted in revised form 20 September 2021. Available online 30 September 2021